Eq. (21) can be rewritten as

$$q(t) = \sum_{i=1}^{\infty}\sum_{j=1}^{\infty}\left(\sum_{m=1}^{M_s}\sum_{n=1}^{N_s}\beta_{ijmn}r_{smn}\right)\eta_{ij}(t) \tag{22}$$

Designating the expected weighting coefficient in Eq. (22) as p_{ij} for the lowest $M_s \cdot N_s$, the z coordinate of the midplane for each sensor segment can be obtained by solving

$$\sum_{m=1}^{M_s}\sum_{n=1}^{N_s}\beta_{ijmn}r_{smn} = p_{ij}$$

$$i = 1, 2, \ldots, M_s, \quad j = 1, 2, \ldots, N_s \tag{23}$$

If some modes in the lowest $M_s \cdot N_s$ modes are not expected to be sensed, the related weighting coefficients are set to be 0. The charge output of the modal sensor might contain the information of the modes whose orders are higher than $M_s \cdot N_s$. However, these high-frequency components in the sensed signal can be easily removed by a low-pass filter.

VII. Results

As an illustrative example, consider a 1 m × 0.7 m × 1 mm simply supported rectangular plate onto which one piezoceramic actuator layer and one piezoceramic sensor are bonded. The actuator and the sensor layers are made of the same lead zirconate titanate (PZT) material, and $e^a_{31} = e^s_{31} = 23.31$ N/Vm. The Young's modulus of the host plate is 210 GPa, and its mass density is 8000 kg/m^3. The first five (11, 21, 12, 31, 22) modes are selected to be controlled by using the modal sensor and the modal actuator. For the modal actuator the constants in Eq. (5) are taken as $A^a_{11} = 1.0$, $A^a_{21} = 0.8$, $A^a_{12} = 0.7$, $A^a_{31} = 0.6$, $A^a_{22} = 0.5$, $A_a = 2.5 \times 10^{-5}$, and $C_a = 0.013$, respectively. The maximum thickness of the modal actuator is less than 0.12 mm, as shown in Fig. 2a. The modal sensor is designed with the parameters $A^s_{11} = 1.0$, $A^s_{21} = 0.7$, $A^s_{12} = 0.6$, $A^s_{31} = 0.5$, $A^s_{22} = 0.4$, $A_s = 3 \times 10^{-5}$, and $C_s = 0$ so that its maximum thickness is less than 0.1 mm, as shown in Fig. 2b. The free vibration of the smart plate is caused by the sudden removal of a force of 3.5 N acted on the point (0.4, 0.3). Using the modal actuator and modal sensor and taking the control gain h in Eq. (13) as 7×10^5, the modal control is performed, and the five controlled modes are shown in Fig. 3. The time history of the central displacement of the plate and control voltage applied on the modal actuator during control are presented in Figs. 4a and 4b, respectively. The results show that all of the target modes of the smart plate have been effectively controlled.

When a pair of uniform actuator and sensor layer with the uniformly distributed control voltage are used to control the simply supported rectangular plate, only the strict odd (for example, 11, 33, 55, etc.) modes can be controllable.[9,10] Thus, modulating the thickness of the sensor and actuator layer can make the control more effective and hence improve the controllability of the structures.

VIII. Conclusions

A new practical method to design the modal actuator/sensor is given for modal control of smart plates by modulating the thickness distribution of the piezoelectric layer. If the stiffness and mass of the piezoelectric layer are considered, the thickness distribution of the modal actuator/sensor can be calculated by an iteration procedure based on a finite element model. In this way the present designing method for modal actuator and modal sensor can be applied to both one-dimensional and two-dimensional structures, such as beams, plates, and shells.

Acknowledgments

The present work was supported by the Australian Research Council under a Large Research Grant (Grant A89905990) and by the National Science Foundation of China (Grant 19802016, 60034010).

References

[1]Meirovitch, L., *Dynamics and Control of Structures*, Wiley-Interscience, New York, 1990.

[2]Lee, C.-K., and Moon, F. C., "Modal Sensors/Actuators," *Journal of Applied Mechanics*, Vol. 57, No. 2, 1990, pp. 434–441.

[3]Gu, Y., Clark, R. L., and Fuller, C. R., "Experiments on Active Control Plate Vibration Using Piezoelectric Actuators and Polyvinylidene Fluoride (PVDF) Modal Sensors," *Journal of Vibration and Acoustics*, Vol. 116, No. 3, 1994, pp. 303–308.

[4]Tzou, H. S., Zhong, J. P., and Hollkamp, J. J., "Spatially Distributed Orthogonal Piezoelectric Shell Actuators Theory and Applications," *Journal of Sound and Vibration*, Vol. 177, No. 3, 1994, pp. 363–378.

[5]Ryou, J.-K., Park, K.-Y., and Kim, S.-J., "Electrode Pattern Design of Piezoelectric Sensors and Actuators Using Genetic Algorithms," *AIAA Journal*, Vol. 36, No. 2, 1998, pp. 227–233.

[6]Sun, D. C., Wang, D. J., and Xu, Z. L., "Distributed Piezoelectric Segment Method for Vibration Control of Smart Beams," *AIAA Journal*, Vol. 35, No. 3, 1997, pp. 583, 584.

[7]Sun, D. C., Wang, D. J., and Xu, Z. L., "Distributed Piezoelectric Element Method for Vibration Control of Smart Plates," *AIAA Journal*, Vol. 37, No. 11, 1999, pp. 1459–1463.

[8]Tzou, H. S., Venkayya, V. B., and Hollkamp, J. J., "Orthogonal Sensing and Control of Continua with Distributed Transducers-Distributed Structronic System," *Dynamics and Control of Distributed Systems*, edited by H. S. Tzou and L. A. Bergman, Cambridge Univ. Press, Cambridge, England, U.K., 1998, pp. 304–370.

[9]Hubbard, J. E., and Burke, S. E., "Distributed Transducer Design for Intelligent Structural Components," *Intelligent Structural Systems*, edited by H. S. Tzou and G. L. Anderson, Kluwer Academic, Norwell, MA, 1992, pp. 305–324.

[10]Sun, D. C., Wang, D. J., Li, Y., and Xu, Z. L., "Stability and Controllability Analysis of Piezoelectric Smart Plates," *Progress in Natural Science*, Vol. 9, No. 6, 1999, pp. 463–471.

A. M. Baz
Associate Editor

Prediction and Design of Metal Plate Vibration Behavior with Bonded Composite Sheets

M. Sasajima,* T. Kakudate,* and Y. Narita†
Hokkaido Institute of Technology, Sapporo 006-8585, Japan

I. Introduction

In practical situations, structural engineers sometimes face the necessity of increasing the stiffness of already existing structures when applied load in actual use exceeds expected design values or the safety standard is strengthened. One recently emerging technique is to bond composite material sheets externally to the existing structures.[1,2] This technique is now widely used in civil engineering structures by making use of its low cost and ease of operation. The authors found in their experiment that this technique is equally applicable to increase static stiffness and strength of metal plates. This reinforcement was effectively made possible to aluminum plates by epoxy adhesive, and the beam under bending showed relatively large deformation without visible debonding of the sheet.

The present Note studies applicability of this technique to designing the maximum natural frequency of metal (aluminum) plates. Theoretically this problem is more complicated than the static optimization, for example, minimizing static deflection, where increase in the bending stiffness is the only consideration. When dynamic

Received 19 July 2001; revision received 1 December 2001; accepted for publication 12 April 2002.

*Graduate Student, Department of Mechanical Engineering, 7-15 Maeda, Teine-ku.

†Professor, Department of Mechanical Engineering, 7-15 Maeda, Teine-ku; narita@hit.ac.jp.

behavior is optimized, for example, maximizing natural frequencies, bonding of extra sheets has two contradicting effects: increasing natural frequencies by stiffening the plate system and decreasing them by adding an extra mass. Moreover, even when the natural frequencies are increased with stiffening effects of bonded sheets, there must be most or nearly optimal location of the sheets that may depend on mode shapes of the plate.

As a plate model, such a partially reinforced plate can be considered as a plate with stepped thickness. Some papers were published dealing with vibration of isotropic plates with stepped thickness (e.g., Ref. 3), but the literature on vibration of isotropic plates partly laminated with composite sheets has not been found because such applications have been impractical in the past.

Based on this new technical demand, the present Note introduces an analysis to study vibration of a rectangular metal (isotropic) plate with bonded unidirectional composite sheets on the surfaces. A Ritz method is used to calculate natural frequencies of the plates with arbitrary boundary conditions. In numerical examples, optimal solutions are sought to design the rectangular plate to yield the maximum fundamental frequency. The location and fiber orientation angle of the bonded sheets are design variables in the optimization. Results are shown to clarify effects of the design variables on increasing or decreasing the fundamental frequencies, and the feasibility is corroborated to obtain the optimized vibration behavior of metal plates by use of bonded composite sheets.

II. Analytical Formulation

Figure 1 shows an isotropic rectangular plate, such as an aluminum plate, that has a pair of unidirectional composite sheets externally bonded on the plate surfaces. The dimension of the base plate is given by $a \times b \times h$ (thickness), and an origin of the global coordinates is located in the center of the plate. Each unidirectional sheet has dimension of $A \times B \times H$ (thickness), and two sheets are symmetrically bonded with an identical fiber orientation angle θ and with the center location at (X, Y) on the surfaces. The location of the sheets is arbitrary on the plate, as long as they stay within the plate region. The sheets are assumed to be perfectly bonded to the base plate.

An analytical method used here is a Ritz method that is chosen due to its simplicity and applicability. The strain energy for the plate system is given in classical plate theory by

$$U = \frac{1}{2}\int (\sigma_x\varepsilon_x + \sigma_y\varepsilon_y + \tau_{xy}\gamma_{xy})\,\mathrm{d}V_P + \frac{1}{2}\int (\sigma_x\varepsilon_x + \sigma_y\varepsilon_y + \tau_{xy}\gamma_{xy})\,\mathrm{d}V_{\mathrm{US}} + \frac{1}{2}\int (\sigma_x\varepsilon_x + \sigma_y\varepsilon_y + \tau_{xy}\gamma_{xy})\,\mathrm{d}V_{\mathrm{LS}} \tag{1}$$

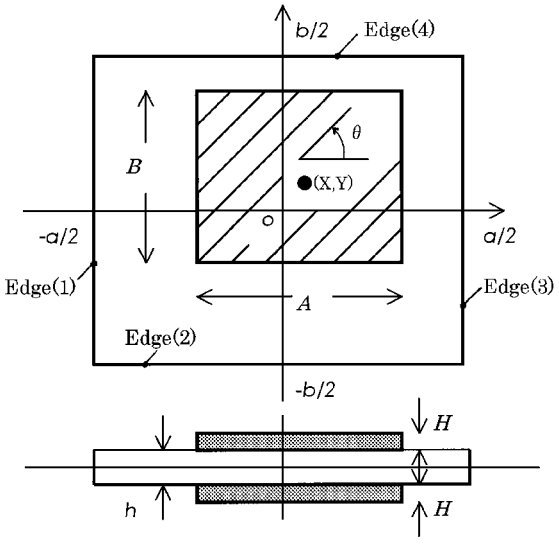

Fig. 1 Rectangular isotropic plate having bonded composite sheets on both surfaces.

where V_P in the first integral is volume of the base plate and V_{US} and V_{LS} in the second and third integrals are the volumes of the upper and lower sheets, respectively. This expression includes both energies due to stretching and bending motions. The bending motion can be uncoupled theoretically from the stretching motion in the present problem because the two sheets are symmetrically bonded, that is, symmetric laminate, with the identical shape and fiber orientation. This allows us to consider only the bending (out-of-plane) vibration that has lower frequency values. After integration along the thickness, the strain energy due to bending is rewritten as

$$U = \frac{1}{2}\int \{K\}[D_{ij}]\{K\}^T\,\mathrm{d}A_P + \frac{1}{2}\int \{K\}\left[D^*_{ij}\right]\{K\}^T\,\mathrm{d}A_{\mathrm{US}} \tag{2}$$

where $\{K\}$ is a curvature vector and $[D_{ij}]$ and $[D^*_{ij}]$ are stiffness matrices given by

$$\{K\} = \left\{-\frac{\partial^2 w}{\partial x^2} \quad -\frac{\partial^2 w}{\partial y^2} \quad -2\frac{\partial^2 w}{\partial x\,\partial y}\right\}$$

$$[D_{ij}] = \begin{bmatrix} D_{11} & D_{12} & 0 \\ D_{12} & D_{22} & 0 \\ 0 & 0 & D_{66} \end{bmatrix}, \qquad \left[D^*_{ij}\right] = 2\begin{bmatrix} D^*_{11} & D^*_{12} & D^*_{16} \\ D^*_{12} & D^*_{22} & D^*_{26} \\ D^*_{16} & D^*_{26} & D^*_{66} \end{bmatrix} \tag{3}$$

where w is deflection of the plate and elements D_{ij} and D^*_{ij} can be determined in an ordinary process.[4] Each element in the stiffness matrix $[D^*_{ij}]$ for the composite sheet is simply doubled due to the symmetric nature of two sheets. The kinetic energy due to bending vibration is defined by

$$T = \frac{1}{2}\left[\int \rho_0\left(\frac{\partial w}{\partial t}\right)^2 \mathrm{d}V_P + \int \rho^*\left(\frac{\partial w}{\partial t}\right)^2 \mathrm{d}V_{\mathrm{US}} + \int \rho^*\left(\frac{\partial w}{\partial t}\right)^2 \mathrm{d}V_{\mathrm{LS}}\right] \tag{4}$$

where ρ_0 and ρ^* are mass per unit volume of the base plate and the bonded sheet, respectively. The maximum strain energy $U_{\max}$ and kinetic energy $T_{\max}$ are obtained by assuming sinusoidal time variation $\sin\omega t$ and redefining w as an amplitude. For simplicity, the nondimensional quantities are introduced as nondimensional coordinates

$$\xi = 2x/a, \qquad \eta = 2y/b \tag{5a}$$

aspect ratio

$$\alpha = a/b \tag{5b}$$

sheet size ratio

$$\delta_x = A/a, \qquad \delta_y = B/b \tag{5c}$$

thickness ratio

$$\bar{h} = H/h \tag{5d}$$

mass ratio

$$\bar{\rho} = \rho^*/\rho_0 \tag{5e}$$

stiffness ratio

$$d_{ij} = D_{ij}/D_0, \qquad \bar{d}_{ij} = D^*_{ij}/D_0 \tag{5f}$$

frequency parameter

$$\Omega = \omega a^2(\rho_0 h/D_0)^{\frac{1}{2}} \tag{5g}$$

and reference stiffness

$$D_0 = \frac{E_0 h^3}{12\left(1-\nu_0^2\right)} \tag{5h}$$

with E_0 and ν_0 being Young's modulus and Poisson's ratio, respectively, of the base plate. The transverse amplitude is assumed by

$$w(\xi,\eta) = \sum_{m=0}\sum_{n=0} C_{mn} X_m(\xi) Y_n(\eta) \tag{6}$$

where C_{mn} are unknown coefficients and the functions X_m and Y_n are

$$X_m(\xi) = \xi^m (\xi+1)^{\mathrm{BC1}} (\xi-1)^{\mathrm{BC3}}$$
$$Y_n(\eta) = \eta^n (\eta+1)^{\mathrm{BC2}} (\eta-1)^{\mathrm{BC4}} \tag{7}$$

where BC1–BC4 are the boundary indices,[5] which are added to satisfy the kinematical boundary conditions (BC) and are used in such a way that $\mathrm{BC}_i = 0$ for free edge (F), 1 for simply supported edge (S), and 2 for clamped edge (C). The integer i denotes edges. (Here $i=1$ is an edge along $\xi=-1$, and edges 2, 3, and 4 are along $\eta=-1$, $\xi=1$, and $\eta=1$, respectively, as shown in Fig. 1.) To the CSFF plate, for instance, $\mathrm{BC}_1=2$, $\mathrm{BC}_2=1$ and $\mathrm{BC}_3=\mathrm{BC}_4=0$ are applied. With these boundary indices BC_i and Eqs. (7), the method of Ritz can accommodate arbitrary sets of the classical BCs.

After minimizing $F = T_{\max} - U_{\max}$ with respect to C_{mn}, one obtains the frequency equation

$$\sum_{m=0}\sum_{n=0}\Big[d_{11} I_1^{(2200)} + \alpha^4 d_{22} I_1^{(0022)} + 4\alpha^2 d_{66} I_1^{(1111)} + \alpha^2 d_{12}\left(I_1^{(0220)} + I_1^{(2002)}\right) + \bar{d}_{11} I_2^{(2200)} + \alpha^4 \bar{d}_{22} I_2^{(0022)} + 4\alpha^2 \bar{d}_{66} I_2^{(1111)} + \alpha^2 \bar{d}_{12}\left(I_2^{(0220)} + I_2^{(2002)}\right) + 2\alpha \bar{d}_{16}\left(I_2^{(1210)} + I_2^{(2101)}\right) + 2\alpha^3 \bar{d}_{26}\left(I_2^{(1012)} + I_2^{(0121)}\right) - \frac{\Omega^2}{16}\left(I_1^{(0000)} + 2\bar{\rho}\bar{h} I_2^{(0000)}\right)\Big]_{,m\bar{m}n\bar{n}} \{C_{mn}\} = 0$$
$$\bar{m} = 0, 1, \ldots, \qquad \bar{n} = 0, 1, \ldots \tag{8}$$

in nondimensional form, where the I are definite integrals that can be evaluated exactly because the integrants are power functions. Equation (8) is a set of linear simultaneous equations in terms of the coefficients C_{mn}, and the eigenvalues Ω may be extracted by using existing computer subroutines.

III. Numerical Results and Discussion

In numerical examples, the isotropic base plate is assumed to be aluminum with material constants of $E_0 = 70.6$ GPa, $\nu_0 = 0.34$, and $\rho_0 = 2700\ \mathrm{kg/m^3}$. The constants for a pair of bonded sheets are $E_L = 138$ GPa, $E_T = 8.96$ GPa, $G_{LT} = 7.1$ GPa, $\nu_{LT} = 0.30$, and $\rho = 1600\ \mathrm{kg/m^3}$ of graphite/epoxy composite.[6] Thus a mass ratio results in $\bar{\rho} = \rho/\rho_0 = 0.6$.

The thickness ratio is taken as $\bar{h} = H/h = 0.1$, where the bonded part is 20% thicker than the base plate. Note that the sheet thickness is considerably thinner than the base plate. The sheet has a square shape and is located at different points: 1, $(X, Y) = (-0.5, 0.5)$; 2, (0, 0.5); 3, (0.5, 0.5); 4, $(-0.5, 0)$; 5, (0, 0); 6, (0.5, 0); 7, $(-0.5, -0.5)$; 8, $(0, -0.5)$; and 9, $(0.5, -0.5)$, as shown in Fig. 2.

A convergence study was made for the frequency parameters Ω_1–Ω_5 (lowest five modes) of the square plate. A pair of bonded sheets have dimension of $\delta_x = \delta_y = 0.5$, where the area of the sheet is a quarter of the base plate, located at the center $(X, Y) = (0, 0)$ on the base plate. The fiber orientation angle within the sheet is $\theta = 30$ deg. The BC of the plate is simply supported along the entire edges (SSSS). The calculated frequencies monotonically decrease from above (upperbound) as the number of terms is increased in Eq. (6) and tend to converge well as $\Omega_1 = 20.08$ (20.08), $\Omega_2 = 49.39$ (49.38), $\Omega_3 = 49.77$ (49.74), $\Omega_4 = 80.20$ (80.19), and $\Omega_5 = 98.97$ (98.97) for $M = N = 10$, where values in the parentheses are for $M = N = 12$. Based on this test result, frequency parameters are calculated hereafter by using the $M \times N = 10 \times 10$ solutions.

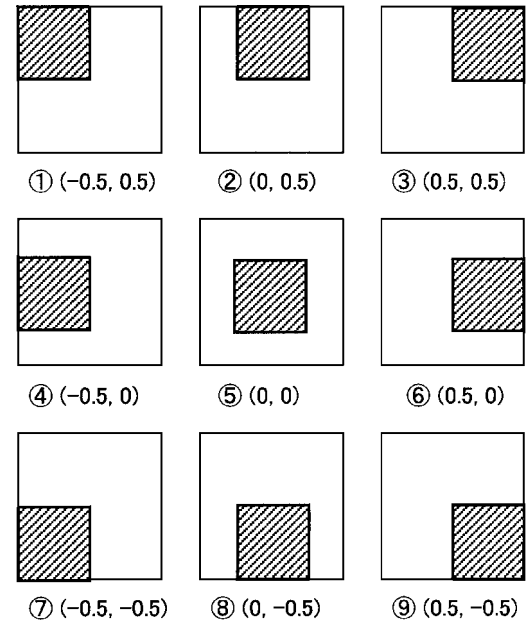

Fig. 2 Location of the square composite sheet on the square base plate in numerical examples.

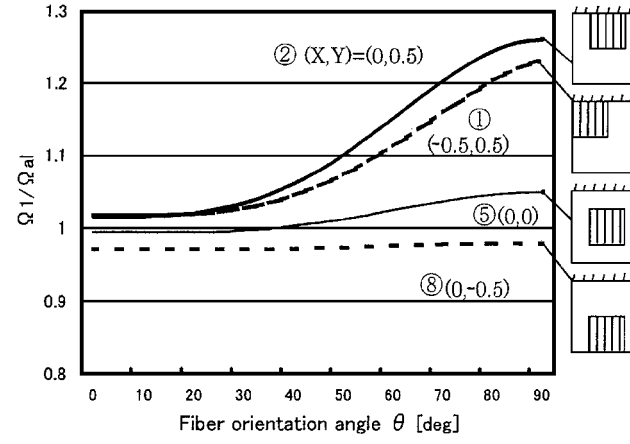

Fig. 3 Ratio of fundamental frequencies Ω_1 of the cantilever plate with sheet to aluminum plate vs the fiber orientation angle θ: $\alpha = 1$ and $\delta_x = \delta_y = 0.5$.

Accuracy of the present solution is also validated by comparing with those of an isotropic stepped plate, that is, a model considered to be a base plate with sheets of the same isotropic material. The present lowest five frequencies are given by $\Omega_1 = 20.59$ (20.43) (Ref. 3), $\Omega_2 = 49.90$ (49.84), $\Omega_3 = 83.16$ (83.36), $\Omega_4 = 105.0$ (105.3), and $\Omega_5 = 106.7$ (105.9) for a simply supported square plate (SSSS) with stepped parts [$\delta_x = \delta_y = 0.25$, $(X, Y) = (0, 0)$]. The present values are in excellent agreement with those of Irie et al.[3] given in the parentheses for all modes.

Figure 3 shows variations of the ratio $\Omega_1/\Omega_{\mathrm{al}}$ where Ω_1 is a fundamental frequency of sheet-bonded plate and Ω_{al} is a fundamental frequency of aluminum plate without sheets. The ratio is plotted vs a fiber orientation angle θ within the bonded sheet ($\delta_x = \delta_y = 0.5$) for a cantilevered square plate (FFFC). The ratios are normalized with respect to an aluminum plate without a bonded sheet to evaluate the effect on frequency variations. If the ratio is more than one, the sheet increases the dynamic stiffness to yield higher frequency, but the sheet has the effect of only adding inertia for $\Omega_1/\Omega_{\mathrm{al}} < 1$ to decrease the frequency.

Among different location of the sheet, the fundamental frequency for sheet 8, $(X, Y) = (0, -0.5)$ at the free end is the lowest and is

Table 1 Ratios of the maximized fundamental frequencies and optimal location and fiber orientation angle of the bonded sheet: $\alpha = 1$ and $\delta_x = \delta_y = 0.5$

BC	Ω_{max}/Ω_{al}	$(X, Y)_{max}$	θ_{max}, deg	Ω_{min}/Ω_{al}
FFFC	1.261	(0, 0.5)	90	0.970
FFSS	1.091	(0.5, 0.5)	135	0.946
FFSC	1.204	(−0.5, 0.5)	82	0.951
FFCC	1.162	(0.5, −0.5)	15	0.954
FSFC	1.098	(0, 0)	90	0.984
FSSS	1.187	(−0.5, 0)	90	0.976
FSSC	1.135	(−0.5, 0)	92	0.973
FSCS	1.137	(−0.5, 0)	90	0.948
FSCC	1.131	(−0.5, 0.5)	87	0.969
FCFC	1.087	(0, 0.5)	90	0.980
FCSC	1.138	(−0.5, 0.5)	90	0.969
FCCC	1.140	(−0.5, 0.5)	90	0.966
SSSS	1.071	(−0.5, 0.5)	45	1.021
SSSC	1.077	(0, 0.5)	90	1.012
SSCC	1.071	(−0.5, −0.5)	135	1.019
SCSC	1.093	(0, 0.5)	90	1.009
SCCC	1.077	(0, 0.5)	90	1.016
CCCC	1.062	(−0.5, 0)	0	1.026

not virtually affected by the change of angle θ. In contrast, a plate with the sheet at root edge 2, $(X, Y) = (0, 0.5)$, gives the highest frequency because the fundamental mode is a simple bending motion with no nodal line, and it is effective to increase the stiffness at the clamped edge in the bending direction ($\theta = 90$). The difference between the maximum and minimum values in Fig. 3 is more than 25%.

Next the fundamental frequencies of the square plate are calculated for 18 different combinations of classical boundary conditions, that is, F, S, and C. There are 21 different combinations of the classical BCs for an isotropic square plate,[7] but the three cases (FFFF, SFFF, and FSFF) involving rigid-body motions are omitted. The optimal fiber orientation angles θ_{max} are searched to give the maximum fundamental frequencies Ω_{max} for nine given sheet locations in Fig. 2, and the frequency ratios Ω_{max}/Ω_{al} ($\Omega_{max} = \text{maximum}\Omega_1$) are tabulated in Table 1. The ratios of the minimum frequency Ω_{min}/Ω_{al} ($\Omega_{min} = \text{minimum}\Omega_1$) are also given at the rightmost column in Table 1.

IV. Summary

Generally, the sets of BCs are listed in the order of increasing edge constraints, starting from FFFC to CCCC, in Table 1. Note that the ratio Ω_{max}/Ω_{al} is higher (the sheet has more stiffening effect) as more free edges are involved. At the same time, however, there exist ratios Ω_{min}/Ω_{al} that are less than one for BCs including at least one free edge. This means that the location of the bonded sheet has a significant effect for plates with more free edges. In contrast, plates strongly constrained along edges (from SSSS to CCCC) are not significantly influenced by addition of bonded composite sheets.

References

[1]Hollaway, L. C., and Leeming, M. B., *Strengthening of Reinforced Concrete Structures: Using Externally-Bonded Frp Composites in Structural and Civil Engineering*, CRC Press, Boca Raton, FL, 1999.

[2]"Inauguration of Nippon Steel Composite," *Nippon Steel News*, No. 274, May/June 1999.

[3]Irie, T., Yamada, G., and Ikai, H., "Natural Frequencies of Stepped Thickness Rectangular Plate," *International Journal of Mechanical Science*, Vol. 22, 1980, pp. 767–777.

[4]Jones, R. M., *Mechanics of Composite Materials*, 2nd ed., Taylor and Francis, Philadelphia, 1999, pp. 190–202.

[5]Narita, Y., Ohta, Y., Yamada, G., and Kobayashi, Y., "Analytical Method for Vibration of Angle-Ply Cylindrical Shells Having Arbitrary Edges," *AIAA Journal*, Vol. 30, No. 3, 1992, pp. 790–796.

[6]Tsai, S. W., *Composite Design*, 4th ed., Think Composites, Dayton, OH, 1998, B-2.

[7]Narita, Y., "Combinations for the Free-Vibration Behaviors of Anisotropic Rectangular Plates Under General Edge Conditions," *Journal of Applied Mechanics*, Vol. 67, 2000, pp. 568–573.

K. N. Shivakumar
Associate Editor

Experimental Nonlinear Response of Tapered Ceramic Matrix Composite Plates to Base Excitation

S. Michael Spottswood*
U.S. Air Force Research Laboratory, Wright–Patterson Air Force Base, Ohio 45433
and
Marc P. Mignolet†
Arizona State University, Tempe, Arizona 85287

Introduction

THE purpose of this investigation was to study the geometric nonlinear response of tapered ceramic matrix composite (CMC) panels to narrowband random loading at several excitation levels. For each loading scenario, the total strain, or combination of bending and axial strain, was recorded at multiple locations along with the axial and bending strain in the panel center. Results of the study will be used to aid in the development of analytical response and fatigue life prediction tools. A second part of this investigation will be dedicated to the failure mode identification of the panels under extreme acoustic and thermal excitation.

The particular CMC material selected has the potential to be used in structurally integrated thermal protection system applications on future hypersonic, transatomospheric, and reusable space vehicles. CMCs represent a class of materials capable of withstanding the intense thermal and acoustic environments such vehicles would experience. This particular CMC is proposed for structures experiencing temperatures in the 871°C (1600°F) range but is representative of room temperature response and failure of brittle matrix composites.

Blevins et al.[1] and Vaicaitis[2] describe the need for new and exotic materials. They note that even unconventional nickel and iron-based superalloys are limited to 982°C (1800°F) before the onset of oxidation and creep. A transatmospheric vehicle will experience the greatest thermal loading in the nose, engine inlet, and nozzle sections with estimated temperatures exceeding 1650°C (3000°F). Furthermore, acoustic loading due to engine noise alone will exceed 170 dB (Ref. 1). This underscores the need for durable composite materials that can withstand these extreme environments. Nonlinear random vibration testing has been accomplished and described in the literature on metallic structures[3–9] and composite materials,[9–12] but further investigations are necessary due to the complex and often unpredictable behavior of composite structures, particularly for unusual geometries such as the asymmetric tapered panel considered here.

Experimental Procedure

This investigation was conducted in the dynamics and acoustics research facility at Wright–Patterson Air Force Base, Ohio. The panels were manufactured from woven nitrided Nextel 312™/Blackglas™ CMC material and were tapered with the minimum thickness in the panel center to reduce the influence of the boundary conditions on the panel failure mode. Figure 1 shows the dimensions of the CMC panel. The panel was a quasi-isotropic layup of 16 plies $(0/90/45/-45/-45/0/90/45)_S$ around the perimeter panel/clamp interface, reduced to 8 plies $(0/45/-45/90)_S$ in the

Received 23 August 2001; revision received 18 March 2002; accepted for publication 18 March 2002; presented as Paper 2002-372 at the AIAA/ASME/ASCE/AHS/ASC 43rd Structures, Structural Dynamics, and Materials Conference, Denver, CO, 22–25 April 2002.

*Aerospace Engineer, Air Vehicles Directorate. Member AIAA.
†Professor, Department of Mechanical and Aerospace Engineering.